Supplemental Material

Rodrigo Berte,[1,2,*] Fabricio Della Picca,[3,*] Martín Poblet,[3] Yi Li,[1] Emiliano Cortés,[1,4] Richard V. Craster,[5] Stefan A. Maier,[1,4,†] and Andrea V. Bragas[3,‡]

[1] *The Blackett Laboratory, Department of Physics, Imperial College London, London SW7 2AZ, United Kingdom*

[2] *CAPES Foundation, Ministry of Education of Brazil, Brasília, DF 70040-020, Brazil*

[3] *Departamento de Física, FCEN, IFIBA CONICET, Universidad de Buenos Aires, Intendente Guiraldes 2160, C1428EGA, Buenos Aires, Argentina*

[4] *Chair in Hybrid Nanosystems, Nanoinstitut München, Fakultät für Physik, Ludwig-Maximilians-Universität München, 80799 München, Germany*

[5] *Department of Mathematics, Imperial College, London SW7 2AZ, UK*

This Supplemental Material contains the description of numerical methods, results of frequency-domain calculations of the in-plane emission pattern of the main modes of nanostructures in Fig. 1, the cross-sections of the rod breathing and disk radial modes in Fig. 2 and the mechanical response of sources of different size for identical receptors in Fig. 3.

FINITE ELEMENT METHOD CALCULATIONS

Numerical calculations were performed by considering a linear elastic response of the isotropic materials and solving Navier's equation in the time- and frequency-domain with either perfectly matched layers (frequency-domain) or low-reflecting (time-domain) boundary conditions:

$$\frac{E}{2(1+\nu)}\left(\frac{1}{(1-2\nu)}\nabla(\nabla\cdot\boldsymbol{u})+\nabla^2\boldsymbol{u}\right)+\boldsymbol{f}=\rho\frac{\partial^2\boldsymbol{u}}{\partial t^2} \tag{S1}$$

where $\boldsymbol{u}$ is the displacement vector, $\boldsymbol{f}$ the force per unit volume, ρ the material density, E the Young's modulus and ν the Poisson's ratio of the material. Continuity of stress and displacement was considered between all boundaries. Time-domain calculations were performed with time intervals $<$ 1ps for a total time of 2.8ns and mesh convergence tested by doubling the number of degrees of freedom solved for until variations in the frequency spectrum of the employed time-domain metric $|\left(\mathcal{F}(\nu)^{n+1}-\mathcal{F}(\nu)^{n}\right)|/\mathcal{F}(\nu)^{n+1} < 0.02$ were obtained for the $n+1$ mesh refinement iteration. Size variations of the nanoantennas were calculated using the displacement at a point at mid-height of the nanostructures. A thermal strain from the increase in the lattice temperature following the electronic relaxation was considered for the displacive excitation mechanism:

$$\varepsilon_{th}=\alpha(T-T_{ref}) \tag{S2}$$

where α is the coefficient of thermal expansion of the nanoparticle, T_{ref} is the reference temperature (set to 293.15 K) and T the lattice temperature.

FAR-FIELD EMISSION PATTERN OF NORMAL MODES

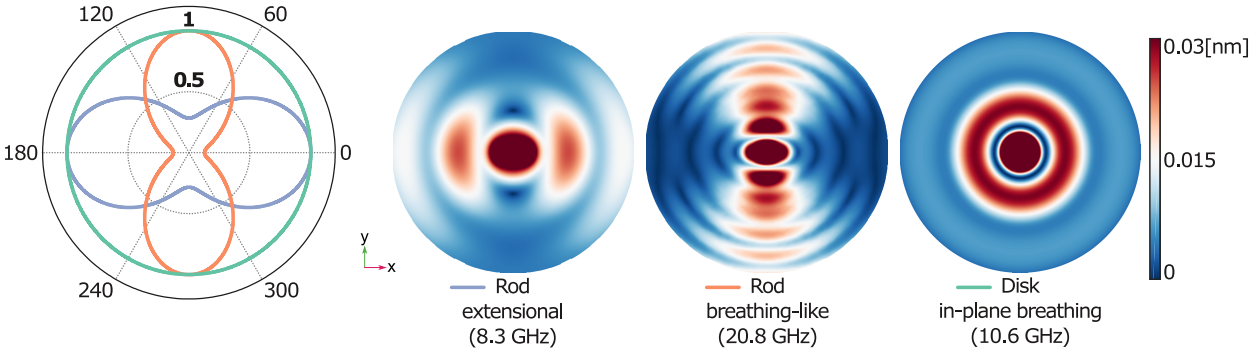

FIG. 1. (left) FEM frequency-domain calculations of the acoustic far-field displacement of rod extensional and breathinglike modes and of disk in-plane radial (breathing) mode. (right) Corresponding substrate displacement, where nanoantennas were omitted for clarity.

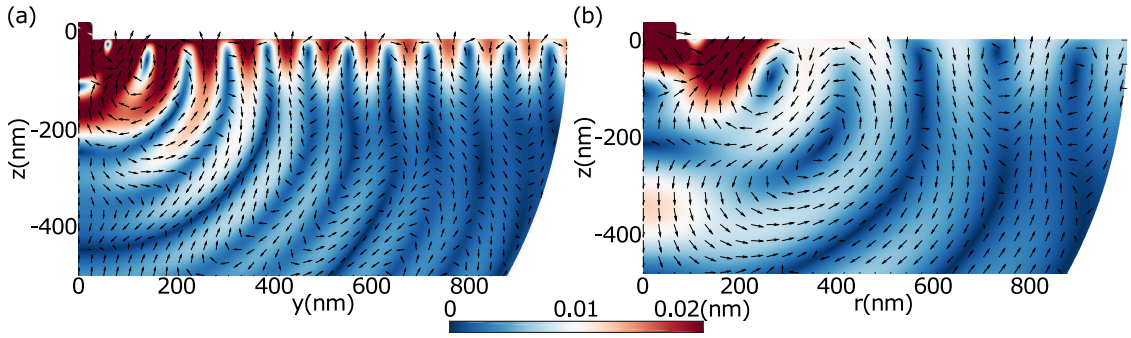

FIG. 2. FEM frequency-domain calculated (a) yz-plane cross-section of displacement (color scale) and polarization (black arrows) of the breathinglike mode of a $140 \times 60 \times 35$ nm Au rod (top left of image) at 20.8 GHz. (b) Radial cross-section of displacement (color scale) and polarization (black arrows) of the in-plane breathing mode of a 140×35 nm Au disk (top left of image) at 10.6 GHz.

SOURCE SIZE EFFECT ON IDENTICAL RECEPTORS

Fig. 3 shows the result of numerical calculations of the effects of sources of different sizes in an identical receptor, both of the same geometry. Using a rod source of varying main-axis size (100, 120 and 140 nm) and a rod receptor of a fixed main-axis size (100 nm), simulations show that although the modes of the source can be probed by the receptor, the eigenmodes of the receptor are as efficiently excited (approximately at 10 GHz), which we attribute to their spectral proximity and identical displacement profiles. Therefore, this particular source-receptor configuration may hamper the accurate determination of the source frequency from the experimental modulated transmitted signals. Such difficulty could be circumvented by choosing a receptor with a well-separated eigenfrequency or different mode displacement profile, such as the disks presented in the main manuscript.

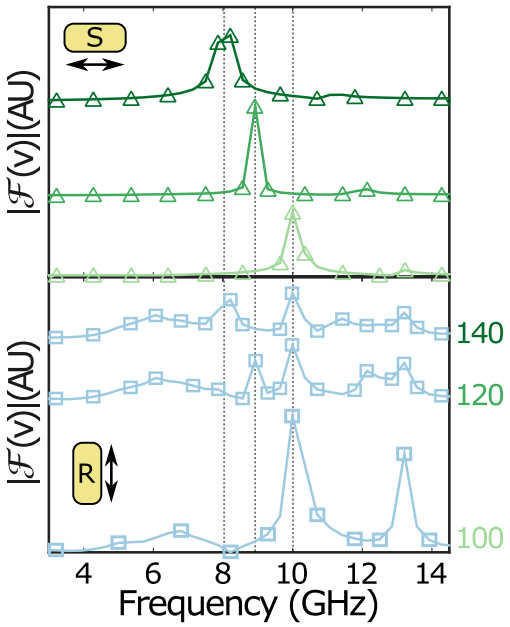

FIG. 3. FEM time-domain Fourier components of the size variation along the axes parallel to the probe beam polarization (black arrows) for rod sources of different size (green - top) and for 100nm rod receptors (blue - bottom). Corresponding source sizes are shown in green on the right hand-side, with stronger colours representing larger sources. Vertical dashed lines correspond to extensional modes of the sources.

* Contributed equally to this work

† Stefan.Maier@physik.uni-muenchen.de

‡ bragas@df.uba.ar